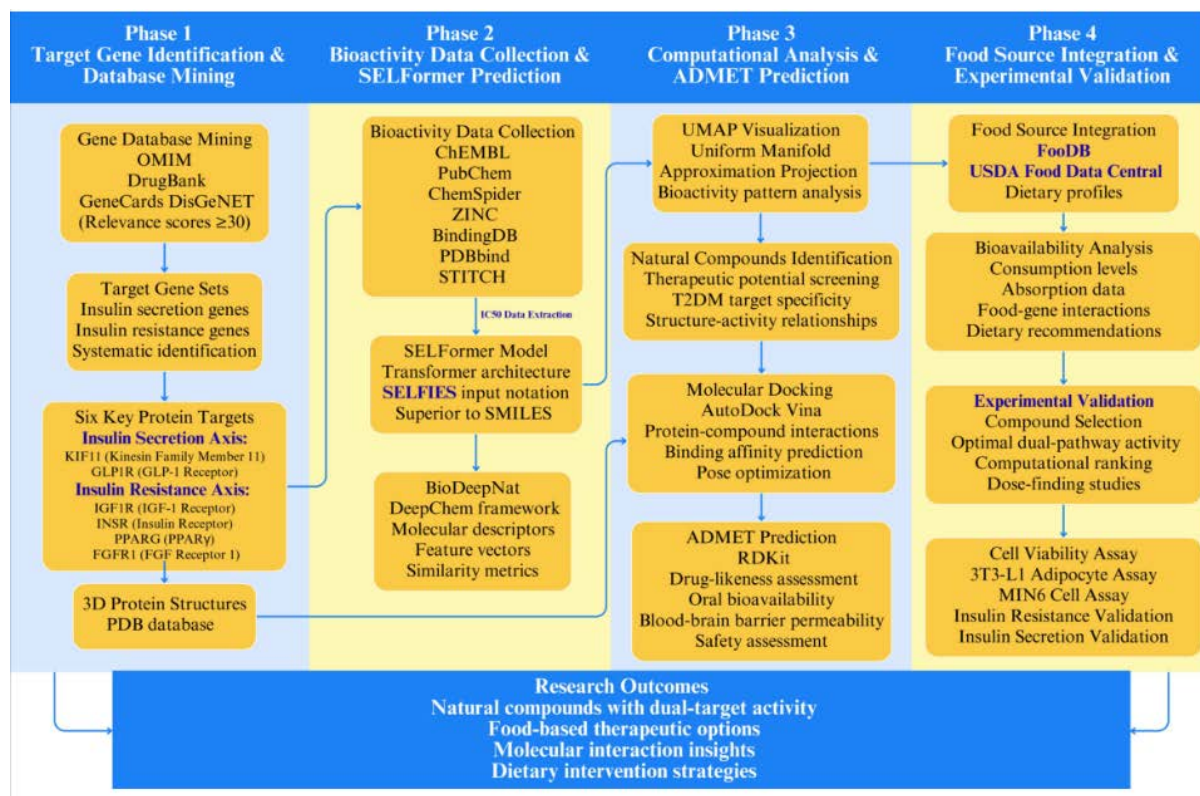
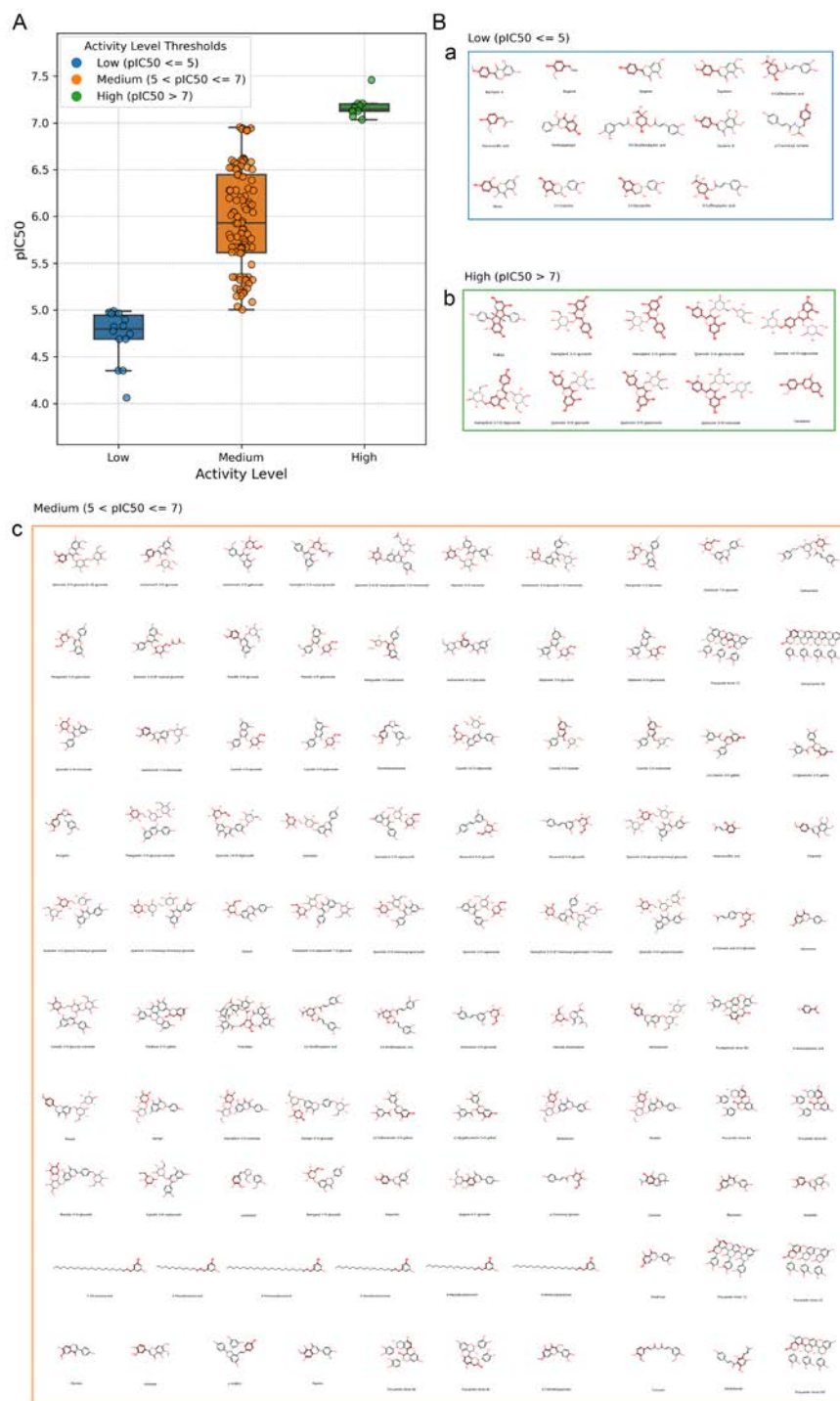


## Supplementary figures



**Figure S1.** Computational Framework for Discovery of Natural Compounds with Therapeutic Potential in T2DM Acting through Modulation of Insulin Secretion and Resistance Pathways. The workflow encompassed four major phases: (1) Target identification and data collection, including gene selection from curated databases and retrieval of IC<sub>50</sub> data; (2) Machine learning prediction, featuring fine-tuning using SELFormer model and prediction of natural compound activity; (3) Natural compound similarity analysis and deep learning classification; (4) Computational analysis, including UMAP visualization, clustering, SAR analysis, and molecular docking studies; Experimental validation through cell-based assays for insulin secretion and resistance, culminating in food source identification for practical dietary applications; and *in vitro* validation.

**Abbreviations:** T2DM, Type 2 diabetes mellitus; IC<sub>50</sub>, Half-maximal Inhibitory Concentration; UMAP, Uniform Manifold Approximation and Projection; SAR, structure activity relationship.



**Figure S2.** Natural Compound Activity Distribution

(A) Histogram plot showing  $pIC_{50}$  values of natural compounds with a threshold line ( $pIC_{50} = 7$ ) separating different active compounds. (B) Chemical structures of representative natural compounds of (a) low-activity, (b) high-activity, and (c) medium-activity.

**Abbreviations:**  $pIC_{50}$ , negative logarithm of the  $IC_{50}$ .

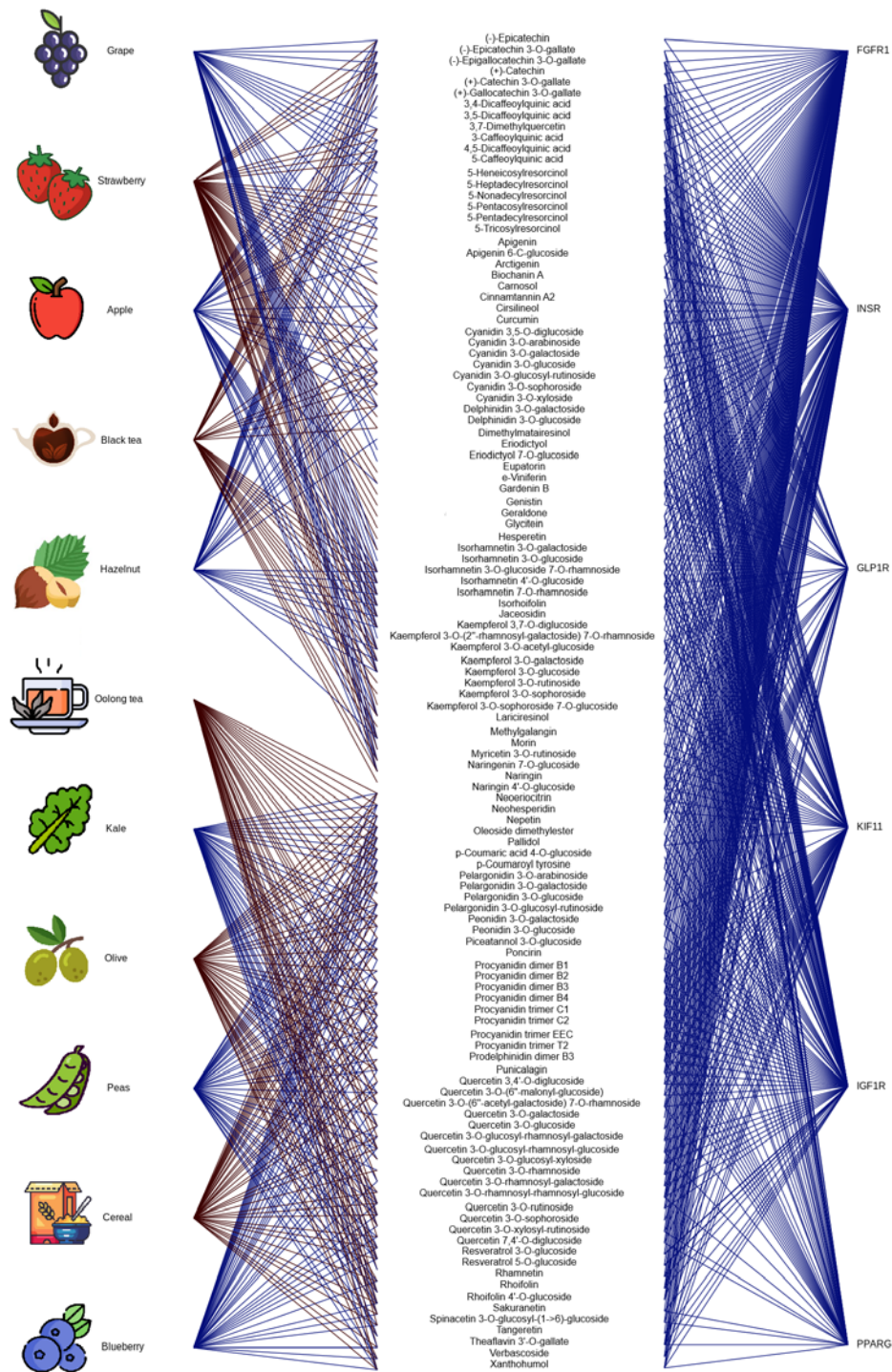


**Figure S3.** Food Source Compound Profiles. Detailed visualization of natural compound profiles across various food sources mentioned in the network analysis. The figure shows the relative abundance and types of bioactive compounds found in strawberries, grapes, tea varieties, and other dietary sources, organized to highlight the richest sources of compounds with therapeutic potential in type 2 diabetes mellitus (T2DM).

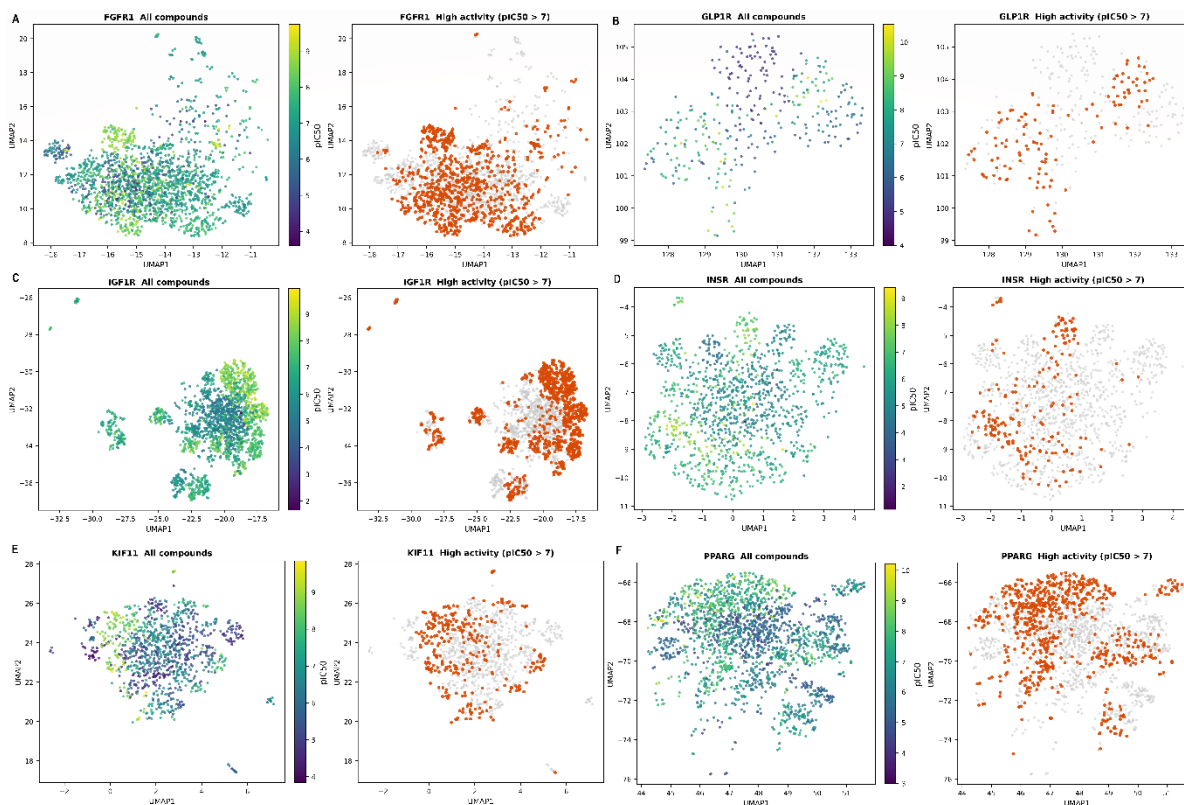
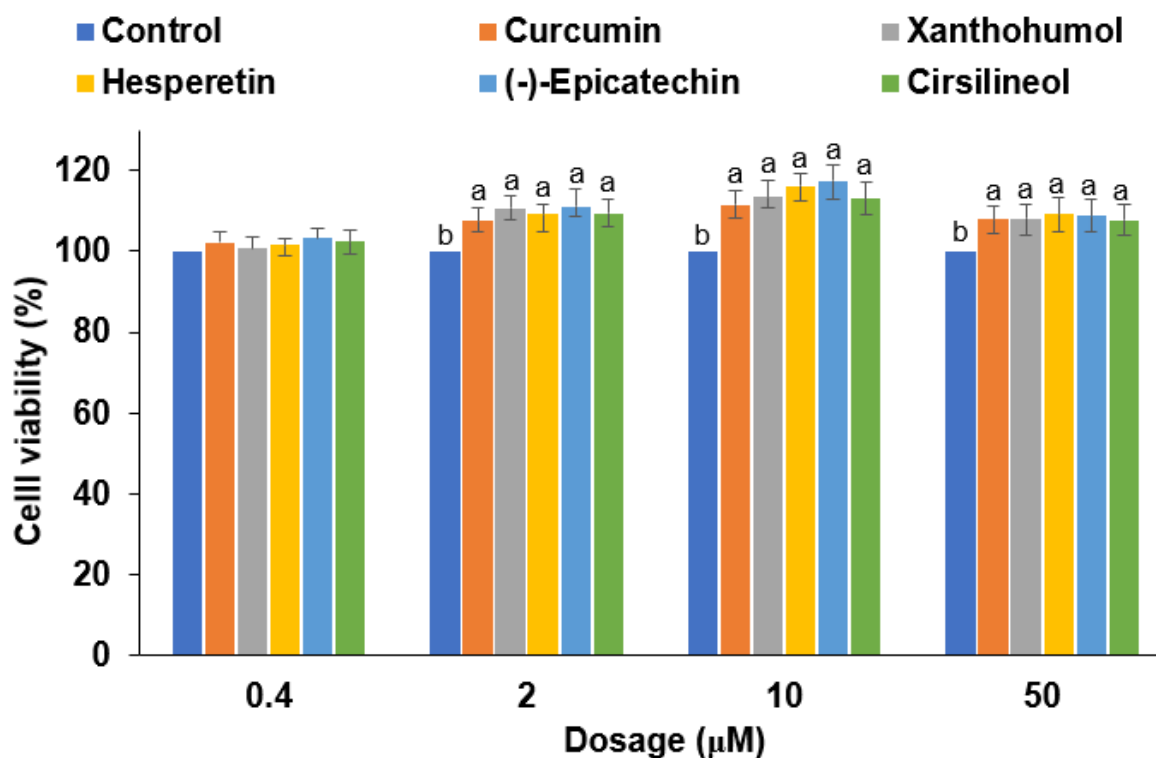


Figure S4. UMAP Visualization Comparing the Full Compound Space and High-Activity Subsets Across Six T2DM-Related Target Proteins.

UMAP projections illustrating the chemical space distribution of all screened compounds (left panels) versus the high-activity subset ( $pIC_{50} > 7$ , right panels) for each of the six T2DM-related target proteins: (A) FGFR1, (B) GLP1R, (C) IGF1R, (D) INSR, (E) KIF11, and (F) PPARG. In the left panels, all compounds are displayed and colored continuously by predicted  $pIC_{50}$  values (viridis scale; purple = low activity, yellow = high activity), revealing the overall bioactivity landscape of the screened chemical space. In the right panels, the full compound set is shown in gray as background reference, with the high-activity subset ( $pIC_{50} > 7$ ) highlighted in red.



**Figure S5. Cell viability assessment of selected natural compounds in 3T3-L1 adipocytes.**

Differentiated 3T3-L1 adipocytes were treated with selected natural compounds at concentrations of 0.4, 2, 10, and 50 μM for 24 hours. Cell viability was assessed using the MTT (3-(4,5-dimethylthiazol-2-yl)-2,5-diphenyltetrazolium bromide) assay. Results are expressed as percentage viability relative to vehicle control (0.1% DMSO, set as 100%). Values represent means ± SD from three independent experiments performed in triplicate. Statistical significance was determined by one-way ANOVA followed by Tukey's post-hoc test for multiple comparisons. Different letters (a, b, c, etc.) indicate statistically significant differences between groups at  $p < 0.05$ .

DMSO, Dimethyl sulfoxide

**Supplementary Table S1.** Individual SELFormer model performance metrics for each T2DM target protein

Target Gene	Pathway	MSE	RMSE	MAE
GLP1R	Insulin Secretion	0.497	0.705	0.311
KIF11	Insulin Secretion	0.853	0.924	0.237
INSR	Insulin Resistance	0.991	0.996	0.603
PPARG	Insulin Resistance	0.884	0.94	0.614
FGFR1	Insulin Resistance	0.88	0.938	0.235
IGF1R	Insulin Resistance	0.993	0.996	0.55

**Supplementary Table S2.** Quantitative comparison of autoencoder variants using Taylor diagram statistics relative to the experimental reference.

Model	Correlation (r)	Standard Deviation ( $\sigma$ )	Centered RMSE (cRMSE)
SimpleAE	0.996	0.924	0.113
ResAE	0.995	0.875	0.158
DeepAE	0.986	0.912	0.180
VAE	0.991	0.737	0.288

**Supplementary Table S3.** Key amino acid residues involved in the interactions between compounds and target proteins.

Target Protein	Compound	Residues involved in hydrogen bonding			Residues involved in hydrophobic interactions					Docking energy, $\Delta G$ (kcal mol <sup>-1</sup> )
		Conventional Hydrogen Bond	Carbon Hydrogen Bond	Alkyl	Pi-Alkyl	Pi-Sigma	Pi-Pi T-shaped	Pi-Donor Hydrogen Bond	Pi-Sulfur	
FGFR1	Curcumin	GLU571,ALA564	No	No	VAL492,LYS514,LEU484	VAL561	No	No	No	-9.54
	Xanthohumol	No	GLU562	No	LEU630,VAL561,ALA640,ILE545	LEU484	PHE489	No	No	-8.664
GLP1R	Xanthohumol	GLN221,TRP214	LEU217	No	ARG299,VAL36,TRP39,TYR88	LEU218	TRP33	No	No	-8.984
IGF1R	Cirsilineol	ARG104,SER187	MET184 , CYS185	No	LEU129	No	No	No	No	-6.766

	Xanthohumol	SER210,THR49,TRP244,ARG77,THR23	TYR225 , CYS221	VAL219,VAL50,ALA220	No	No	TRP244	No	No	-7.632
KIF11	Xanthohumol	ASN287	GLY296,LEU293,THR300	ILE332,ALA356,ALA53,VAL21,ALA334	No	TYR104 , LEU292	No	No	No	-9.393
	Xanthohumol	LEU1002,ARRG1000,SE R1090	ALA1080	MET1139,LEU1002	No	No	No	No	No	-7.727
INSR	Cirsilineol	ASP1150,LEU1002	MET1079,ALA1080	No	MET1139,ALA1028,VAL1010,LEU1002	No	No	No	No	-7.713
PPARG	Xanthohumol	GLU343,SE R342	No	No	CYS285,PH E287	ARG288	TYR327	HIS449	MET364	-8.425